# A Comparative Study of Meshless Approximations in Local Integral Equation Method

**Vladimir Sladek[1], Jan Sladek[1] and Chuanzeng Zhang[2]**

**Abstract:** This paper concerns the stability, convergence of accuracy and cost efficiency of four various formulations for solution of boundary value problems in non-homogeneous elastic solids with functionally graded Young's modulus. The meshless point interpolation method is employed with using various basis functions. The interaction among the elastic continuum constituents is considered in the discretized formulation either by collocation of the governing equations or by integral satisfaction of the force equilibrium on local sub-domains. The exact benchmark solutions are used in numerical tests.

**keyword:** Integral equation method, Integral force equilibrium, Collocation method, Point interpolation method, Radial basis functions, Elasticity, Functionally Graded Materials (FGMs)

## 1 Introduction

Complying with general physical principles, the standard computational methods, such as the FDM (based on direct discretization of the governing equations) and FEM (formulation based on global variational principles), serve as versatile tools in numerical solution of boundary value problems (BVP) for field equations in various continua theories. The use of finite size elements is a physically reasonable methodology, since the mesh based methods with polynomial interpolation within the elements exhibit convergence of accuracy of numerical results to exact solutions with mesh refinement. The mesh reduction is achieved in the boundary integral equation method (BIEM), since the unknowns are localized on the boundary alone because of the utilization of the fundamental solutions of governing equations in this semi-analytical method. Nevertheless, there

are some shortcomings of these methods in some applications. First of all, since the mesh generation is not fully automated, some difficulties may appear in solving problems with free or moving boundary when re-meshing is required. Another difficulty appears in problems with large distortions of discretization elements or separation of the continuum especially in fluid problems. The pure boundary formulation fails if the fundamental solution is not available.

A great attention is paid to the research of meshless methods, since there are still problems to be solved. The amount of applications of meshless methods is also increased rapidly giving either solutions of new problems or comparisons in accuracy and efficiency with standard methods. Meshless methods can be categorized into two major categories [Liu (2003)]: (i) strong-form meshless methods (based on meshless approximation and collocation of the governing equations); (ii) weak-form meshles methods (based on meshless approximation and integral treatment of the governing equations). Each of the approaches has its own advantages as well as shortcomings. The strong-form methods are truly meshless and simple to implement. However, they are often unstable and less accurate. On the other hand, weak-form meshless methods based on global formulations are not truly mesh-free because the background mesh is required for integration over the analysed domain. Recently, Atluri and his co-workers presented a family of robust truly meshless methods based on the local weak Petrov-Galerkin formulation for the solution of boundary value problems governed by arbitrary partial differential equations (see e.g. [Atluri and Shen (2002), Atluri (2004)]). Depending on the choice of the test and the trial functions, the Meshless Local Petrov-Galerkin (MLPG) method results in various meshless formulations for both domain and boundary-integral equations of PDEs. These methods have certain advantages over the mesh-based FEM and BEM in many currently available computer codes.

The meshless weak-form methods exhibit better stability

[1] Institute of Construction and Architecture, Slovak Academy of Sciences, 845 03 Bratislava, Slovakia,,E-mail: vladimir.sladek@savba.sk, jan.sladek@savba.sk
[2] Department of Civil Engineering, University of Siegen, D-57068 Siegen, Germany E-mail: c.zhang@uni-siegen.de

and accuracy. On the other hand, the numerical evaluation of shape functions at the integration points is very time consuming. The advantages of both the weak and strong meshelss formulations tried to utilize Liu and Gu in their meshfree weak-strong form method [Liu et al (2003)]. The weak-form is applied on the Neumann part of the boundary with prescribed natural boundary conditions, while on the rest of the body the strong-form is applied with decreasing the amount of integration points dramatically.

Much effort has also been devoted to the development of new interpolation techniques. An overview of the meshless approximations can be found in the books [Atluri and Shen (2002), Atluri (2004)]. The widely used classical radial basis functions (RBFs) give good convergence in strong formulations only at the cost of instability. Then, domain decomposition and regularization are required [Zhou et al (2003)]. Another drawback is a high sensitivity on the selection of the shape parameter values [Xiao et al (2003), Rippa (1999), Wang et al (2002)]. In the local point interpolation method (PIM) [Liu and Gu (2001), Liu (2003)] a set of points is used to approximate a field variable in a neighborhood of a point.

In the present study, we concern with the stability, convergence of accuracy and cost efficiency of four various formulations for solution of boundary value problems (BVP) in non-homogeneous elastic solids with functionally graded Young's modulus. For meshless implementations we shall use PIM based on: (i) classical RBFs; (ii) compactly supported RBFs with assuming the radius of the support domain as the shape parameter [Xiao (2004)]; (iii) combination of polynomials and multiquadrics. The interpolation functions possess the Kronecker delta property, hence the degrees of freedom (DOFs) are nodal values of displacements. Each approximation point is associated with a center of approximation which is a nodal point. Thus, savings in the CPU-time are achieved. The Dirichlet (essential) boundary conditions are considered via collocation and the Neumann (natural) boundary conditions either via collocation or by the integral force equilibrium on local sub-domain. The interaction among the DOFs is considered either in strong form (by collocation of the governing equations at interior nodes) or in a weak form (by satisfaction of the force equilibrium on local sub-domains). In numerical tests we consider such examples for which exact solutions are available. The numerical results are obtained also for the LIE formulation

implemented by the approximation on standard quadrilateral quadratic elements. The cost efficiency is assessed by the CPU times.

## 2  Integral equation formulation

In the case of elastic bodies under static loadings conditions, the governing equations are given by the force equilibrium which is written in the differential form as

$$\sigma_{ij,j}(\mathbf{x}) + X_i(\mathbf{x}) = 0, \quad \text{in } \Omega, \tag{1}$$

where $\sigma_{ij}$ is the stress tensor due to cohesive forces as a response to external loadings and $X_i(\mathbf{x})$ is the density of body forces. The relationship between the inherent forces and deformations of the linear elastic continuum is given by the generalized Hooke's law

$$\sigma_{ij}(\mathbf{x}) = c_{ijkl}(\mathbf{x}) u_{k,l}(\mathbf{x}), \tag{2}$$

where $u_k(\mathbf{x})$ are the Cartesian components of the displacement field and the tensor of material coefficients may be position dependent in non-homogeneous media. In the case of isotropic media, it is defined only by two coefficients, e.g. the Young modulus $E(\mathbf{x})$ and the Poisson ratio $\nu$ which is usually constant. Then, the constitutive law can be written as

$$c_{ijkl}(\mathbf{x}) = E(\mathbf{x}) c_{ijkl}^o \quad,$$
$$c_{ijkl}^o = \frac{1}{2(1+\nu)} \left( \delta_{ik}\delta_{jl} + \delta_{il}\delta_{jk} + \frac{2\overline{\nu}}{1-2\overline{\nu}}\delta_{ij}\delta_{kl} \right), \tag{3}$$

where the new parameter $\overline{\nu}$ is defined by the Poisson ratio as

$$\overline{\nu} = \begin{cases} \nu/(1+\nu), & \text{for plane stress conditions} \\ \nu, & \text{otherwise} \end{cases}. \tag{4}$$

Finally inserting (3) and (2) into (1), we obtain the governing PDE for the displacements

$$E(\mathbf{x}) c_{ijkl}^o u_{k,lj}(\mathbf{x}) + E_{,j}(\mathbf{x}) c_{ijkl}^o u_{k,l}(\mathbf{x}) = -X_i(\mathbf{x}) \quad. \tag{5}$$

The standard boundary conditions prescribe either the displacements or tractions on the Dirichlet and Neumann part of the boundary, respectively

$$u_i(\eta) = \tilde{u}_i(\eta) \text{ at } \eta \in \partial\Omega_D,$$
$$n_j(\eta) c_{ijkl}(\eta) u_{k,l}(\eta) = \tilde{t}_i(\eta) \text{ at } \eta \in \partial\Omega_N. \tag{6}$$

The fundamental solution for the governing equation is defined as the solution of Eq. (5) due to the point forces $X_i(\mathbf{x}) = \delta_{im}\delta(\mathbf{x} - \mathbf{y})$, $(m = 1, \ldots, d)$ in an infinite space with the dimensionality $d$. Apparently, the fundamental solution of the PDE with variable coefficients is not available in closed form in the case of general material non-homogeneity. Consequently, the pure boundary formulation based on integral equations is not available. It seems that each numerical solution of BVP in elastic media with arbitrary non-homogeneity should utilize both the boundary and interior degrees of freedom.

Assuming a certain domain-type approximation for field variables, one can evaluate also approximated gradients and/or higher order derivatives of field variables. Thus, prescribed boundary conditions can be recast into discretized equations and what we need is to find proper relationships among the nodes. These can be obtained either in local form by simple collocation of the governing PDEs at nodal points (strong form) or in integral form by integrating the governing PDE over local sub-domains $\Omega^c \subset \Omega$ (weak form). The latter is a reverse way of the derivation of the governing PDEs from the general physical balance principles of a continuum theory where such principles take the form of integral equations holding for all arbitrary but small material domains $\Omega^c$. Thus, integration of Eq. (1) leads to

$$\int_{\Omega^c} \sigma_{ij,j}(\mathbf{x}) d\Omega(\mathbf{x}) = -\int_{\Omega^c} X_i(\mathbf{x}) d\Omega(\mathbf{x}). \tag{7}$$

By applying the Gauss divergence theorem to Eq. (7) and bearing in mind the definition of tractions $t_i = \sigma_{ij}n_j$, we obtain an integral form of the balance principle as

$$\int_{\partial\Omega^c} t_i(\eta) d\Gamma(\eta) = -\int_{\Omega^c} X_i(\mathbf{x}) d\Omega(\mathbf{x}) \quad \text{or}$$

$$\int_{\partial\Omega^c} n_j(\eta) c_{ijkl}(\eta) u_{k,l}(\eta) d\Gamma(\eta) = -\int_{\Omega^c} X_i(\mathbf{x}) d\Omega(\mathbf{x}), \tag{8}$$

where $n_j(\eta)$ denotes the Cartesian components of the unit outward normal vector at $\eta$ on the boundary $\partial\Omega^c$ of the sub-domain $\Omega^c$. Eq. (8) is the integral expression of the force equilibrium in an arbitrary material domain $\Omega^c$. Hence, it is a physically admissible constraint that can be used as a coupling equation in the computation of the unknown DOF of the discretized problem. Recall that the local integral equations (8) are non-singular, since there are no singular fundamental solutions involved in contrast to the singular integral equations employed in the boundary integral equation method.

## 3 Meshless approximations of field variables

Let the displacements $u_i(\mathbf{x})$ be approximated within a sub-domain $\Omega_s \subset (\Omega \cup \partial\Omega)$. If both $\Omega_s$ and $\Omega$ have the same dimension, then we call the approximation as a domain-type approximation. One of the possibilities to achieve a domain-type approximation is to use standard finite size domain elements like in FEM which of course is not a meshless approximation [Sladek et al (2005b)].

In all meshless approximation techniques, shape functions have to be defined for the approximation of the field variable $u_i(\mathbf{x})$ within a sub-domain $\Omega_s$ using only nodes scattered arbitrarily in the analyzed domain without any predefined mesh to provide a connectivity of the nodes. Assuming a finite series representation of the field variable in a sub-domain $\Omega^q$ surrounding the nodal point $\mathbf{x}^q$, the approximated field can be written as

$$u_i(\mathbf{x})|_{\Omega^q} = \sum_{a=1}^{N^q} B^{(q,a)}(\mathbf{x}) c_i^a(\mathbf{x}^q) \tag{9}$$

where $B^{(q,a)}(\mathbf{x})$ are the basis functions defined in the Cartesian coordinate space, $N^q$ is the number of nodes in the support domain of the point $\mathbf{x}^q$, and $c_i^a(\mathbf{x}^q)$ are the expansion coefficients at a given point $\mathbf{x}^q$.

In this paper, we shall pay attention to Point Interpolation Methods (PIM) [Liu (2003)] based on using either pure radial basis functions (RBFs) of various kinds [PIM(RBF)] or a combination of polynomials and multiquadrics taken as RBFs [PIM(P+RBF)]. The displacement field is interpolated within $\Omega^q$ in terms of its nodal values and certain shape functions. Then, the DOFs of the discretized domain-type formulation are given by the nodal values of displacements. The boundary conditions and the interaction among the DOFs can be satisfied approximately by spreading a sufficient amount of knots on the global boundary and in the interior of the analyzed domain. Since in most engineering applications, a complete solution throughout the analyzed domain is needed, the use of domain-type approximations could be efficient because of simple and low cost post-processing calculations.

### 3.1 Meshless PIM(RBF)

The radial basis functions are defined as $g^q(\mathbf{x}) = g(|\mathbf{x} - \mathbf{x}^q|)$ with $\mathbf{x}^q \in \Omega^q \subset \Omega$. Let the interpolation domain around the nodal point $\mathbf{x}^q$, $\Omega_i^q$, be defined as a circle with the radius $r_i(\mathbf{x}^q)$. Then, the number of nodes involved in $\Omega_i^q$ is given as

$$N^q = \sum_{a=1}^{N_t} H\left(r_i(\mathbf{x}^q) - |\mathbf{x}^a - \mathbf{x}^q|\right),$$

where $H(z)$ is the Heaviside unit step function and $N_t$ is the total number of nodes. Let $n(q,a)$ be the global number of the $a$-th local node among the $N^q$ nodes adjacent to the node $\mathbf{x}^q$. If $|\mathbf{x} - \mathbf{x}^q| = \min_{\forall a} |\mathbf{x} - \mathbf{x}^a|$, we shall assume the approximation of displacements at $\mathbf{x} \in \Omega^q$ as

$$u_i(\mathbf{x}) \approx \sum_{a=1}^{N^q} \alpha^a g\left(\left|\mathbf{x} - \mathbf{x}^{n(q,a)}\right|\right) \quad . \tag{10}$$

The node $\mathbf{x}^q$ will be called as center of approximation for approximation at $\mathbf{x} \in (\Omega \cup \partial\Omega)$.

Hence,

$$u_i(\mathbf{x}^{n(q,b)}) = \sum_{a=1}^{N^q} g^{ba}\alpha^a, \quad g^{ba} = g\left(\left|\mathbf{x}^{n(q,b)} - \mathbf{x}^{n(q,a)}\right|\right)$$

and finally,

$$u_i(\mathbf{x}) = \sum_{a=1}^{N^q} u_i(\mathbf{x}^{n(q,a)})\varphi^{(q,a)}(\mathbf{x}),$$

$$\varphi^{(q,a)}(\mathbf{x}) = \sum_{b=1}^{N^q} (\mathbf{g}^{-1})^{ba} g\left(\left|\mathbf{x} - \mathbf{x}^{n(q,b)}\right|\right). \tag{11}$$

Thus, the displacement field in $\Omega^q$ is approximated in terms of nodal values and the shape functions $\varphi^{(q,a)}(\mathbf{x})$. Recall that in the case of RBFs the inverse matrix $\mathbf{g}^{-1}$ is non-singular and $\varphi^{(q,a)}(\mathbf{x}^{n(q,b)}) = \delta_{ab}$. Since the inverse moment matrices can be computed in advance and can be employed properly in evaluation of the shape function after finding the center of approximation for an arbitrary point $\mathbf{x} \in (\Omega \cup \partial\Omega)$, it is not needed to compute such matrices repeatedly at each approximation point what results in certain savings in the CPU-times.

As regards the choice of the RBFs, we shall consider various kinds including:

(i) Multiquadrics (MQ) [Hardy (1990)] : $g(r) = \left((r/L)^2 + (s/L)^2\right)^m$, $r = |\mathbf{x} - \mathbf{x}^q|$, $m = 1/2$

(ii) Gaussian: $g(r) = e^{-(sr/L^2)^2}$

(iii) Duchon's Thin Plate Splines (TPS): $g(r) = (r/L)^2 \ln((r+s)/L)$

*compactly supported RBFs*

(iv) Wendland C2: $g(r) = (1 - r/s)_+^4 (4r/s + 1)$

(v) Wendland C4: $g(r) = (1 - r/s)_+^6 (35(r/s)^2 + 18r/s + 3)$

(vi) Wu C4: $g(r) = (1 - r/s)_+^6 (5(r/s)^5 + 30(r/s)^4 + 72(r/s)^3 + 82(r/s)^2 + 36r/s + 6)$,

where the radius of support domain $s$ is considered as the shape parameter and

$$(\cdot)_+ = \begin{cases} (\cdot), & if \ (\cdot) \geq 0 \\ 0, & if \ (\cdot) < 0 \end{cases}$$

and $L$ is a length parameter.

### 3.2 Meshless PIM(P+RBF)

The use of polynomials as the basis functions in PIM exhibits many excellent properties with respect to the consistency and accuracy of the method, as long as the moment matrix is invertible [Liu (2003)]. Unfortunately, the singularity of the moment matrix is dependent on the nodal points distribution. In [Liu (2003)], several techniques have been proposed to avoid a singular moment matrix. One way to avoid singular moment matrix in the polynomial PIM is to use a radial-polynomial basis [Liu (2003), Sladek et al (2005a)]. Then,

$$u_i(\mathbf{x})|_{\Omega^q} = \sum_{a=1}^{N^q} R^{n(q,a)}(\mathbf{x})\alpha_i^{(q,a)} + \sum_{a=1}^{M} P^a(\mathbf{x})\beta_i^{(q,a)}, \tag{12}$$

where $N^q$ is determined as in previous subsection and $M < N^q$ is the number of monomials. The choice $M = 6$ corresponds to the utilization of a complete quadratic polynomial basis

$$P^a(\mathbf{x}) \in \left\{1, r_1, r_2, r_1 r_2, r_1^2, r_2^2\right\}, \quad r_i = x_i - x_i^q, \tag{13}$$

while the RBFs are chosen as multiquadrics

$$R^n(\mathbf{x}) = \left(|\mathbf{x} - \mathbf{x}^n|^2 + s^2\right)^m, \quad m = 1/2. \tag{14}$$

Collocating eq. (12) at $\mathbf{x}^{n(q,b)}$

$$R^{bj}\alpha_i^j + P^{bj}\beta_i^j = u_i^b, \quad (b = 1, ..., N^q),$$

$$R^{bj} = R^{n(q,j)}(\mathbf{x}^{n(q,b)})$$

and assuming an additional condition

$$\alpha_i^m P^{ma} = 0, \quad (a = 1, \ldots, M), \quad P^{ba} = P^a(\mathbf{x}^{n(q,b)}),$$

one can get the expression for approximation of displacements in term of nodal values and shape functions

$$u_i(\mathbf{x})|_{\Omega^q} = \sum_{a=1}^{N^q} u_i(\mathbf{x}^{n(q,a)}) \varphi^{(q,a)}(\mathbf{x}).$$

with the explicit expression for the shape functions being given elsewhere [Sladek et al (2005a)]. The Kronecker-delta property is satisfied once again.

Once having a domain-type approximation of displacements, one can get also the approximations for derivatives of displacements

$$u_{i,j}(\mathbf{x})|_{\Omega^q} = \sum_{a=1}^{N^q} u_i(\mathbf{x}^{n(q,a)}) \varphi_{,j}^{(q,a)}(\mathbf{x}),$$

$$u_{i,jk}(\mathbf{x})|_{\Omega^q} = \sum_{a=1}^{N^q} u_i(\mathbf{x}^{n(q,a)}) \varphi_{,jk}^{(q,a)}(\mathbf{x}), \tag{15}$$

which are expressed in terms of the nodal values of displacements and the derivatives of the shape functions.

## 4 Discretized equations

In view of the Kronecker-delta property of the shape functions, it is very simple to implement the prescribed boundary conditions on the Dirichlet part of the boundary

$$u_i(\mathbf{x}^c) = \tilde{u}_i(\mathbf{x}^c) \text{ at } \mathbf{x}^c \in \partial\Omega_D, \tag{16}$$

while on the Neumann part, we can consider two alternatives.

*B-1. Collocation of the prescribed tractions* (strong-form method)

$$n_j(\mathbf{x}^c) c_{ijkl}(\mathbf{x}^c) \sum_{a=1}^{N^c} u_k(\mathbf{x}^{n(c,a)}) \varphi_{,l}^{(c,a)}(\mathbf{x}^c) = \tilde{t}_i(\mathbf{x}^c)$$

$$\text{at } \mathbf{x}^c \in (\partial\Omega_N - \partial\Omega_D). \tag{17a}$$

*B-2. Integral treatment of traction (natural) conditions* (weak-form method)

In view of Fig. 1 with assuming the body forces to be absent, we may write the integral form for the force equilibrium as

$$c_{ijkl}^o \sum_{a=1}^{N^c} u_k(\mathbf{x}^{(c,a)}) \int_{L^c} n_j(\eta) \varphi_{,l}^{(c,a)}(\eta) d\Gamma = -\int_{\Gamma_N^c} \tilde{t}_i(\eta) d\Gamma.$$

$$\tag{17b}$$
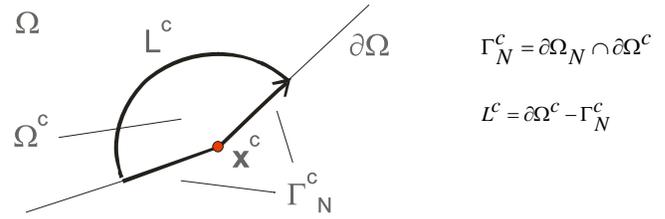


**Figure 1** : Sketch of the boundary node on the Neumann part of the global boundary $\partial\Omega_N \subset \partial\Omega$

Now, the physical information about the boundary conditions is recast into the discretized formulation for solution of the BVP by collocation of the boundary conditions with using the approximation of the field variables and what we need, is to introduce coupling among the DOFs in a physically correct way. We shall consider two alternatives for incorporation of this interaction.

*I-1. Collocation of the governing PDEs* (strong-form method)

Taking into account the approximations given by eq. (15), we can discretize the PDE (5) collocated at interior nodes $\mathbf{x}^c$ as

$$c_{ijkl}^o \sum_{a=1}^{N^c} u_k(\mathbf{x}^{n(c,a)}) \left[ E(\mathbf{x}^c) \varphi_{,lj}^{(c,a)}(\mathbf{x}^c) + E_{,j}(\mathbf{x}^c) \varphi_{,l}^{(c,a)}(\mathbf{x}^c) \right]$$

$$= -X_i(\mathbf{x}^c) = 0. \tag{18}$$

Although there is no integration in this approach, the second derivatives of the shape functions are needed. There exists a trade-off principle which says that good convergence can only be achieved at the cost of instability. To overcome this problem, one can either use domain decomposition to subdivide the global problem into smaller systems of equations [Zhou et al (2003)] or to use compacted supported RBFs with effectiveness supports. Another expected drawback in classical RBFs is the selection of shape parameters.

*I-2. Integral equations on local sub-domains* (weak-form method)

One may choose arbitrarily the size and shape of sub-domains on which the integral form of force equilibrium is considered. Nevertheless, one aims to choose the size of the interpolation domains much smaller than the size of the global domain, in order to get a sparse system matrix of the discretized equations. Furthermore, the size of the sub-domains should be much smaller than the size of the interpolation domains to achieve stability of the approximation on sub-domains. Therefore we select a small circular sub-domain $\Omega^c$ around each interior node $\mathbf{x}^c$ with $\Omega^c \subset \Omega$. Then, the local integral equation collocated at an interior node $\mathbf{x}^c$ is given as

$$c^o_{ijkl} \sum_{a=1}^{N^c} u_k(\mathbf{x}^{(c,a)}) \int_{\partial \Omega^c} n_j(\eta)\varphi^{(c,a)}_{,l}(\eta)d\Gamma = 0, \qquad (19)$$

where the integration over the circular boundary $\partial \Omega^c$ can be performed very easily. The localization of the integration on the boundary of the sub-domain yields a significant reduction of the number of integration points and finally also the portion of the computational time spent by evaluation of the shape functions at integration points.

## 5   Numerical examples

In order to test the proposed numerical methods, we consider examples for which analytical solutions are available. The body forces are vanishing in $\Omega$, the Poisson ratio is constant $\nu = 0.25$, plane stress conditions are assumed and the gradation of the Young modulus is given by a prescribed function $E(\mathbf{x}) = E_o f(\mathbf{x})$.

In the study of the convergence and accuracy of the numerical results with respect to the increasing density of nodal points, we use the global % error defined as

$$\text{GPE} = 100 \left\{ \sum_{a=1}^{N_t} \Delta u_i^a \Delta u_i^a \right\}^{1/2} / \left\{ \sum_{a=1}^{N_t} u_i^{ex}(\mathbf{x}^a) u_i^{ex}(\mathbf{x}^a) \right\}^{1/2},$$

$$\Delta u_i^a = u_i^{num}(\mathbf{x}^a) - u_i^{ex}(\mathbf{x}^a) \quad, \qquad (20)$$

where $N_t$ is the total number of nodes on the closed domain $\Omega \cup \partial \Omega$.

In most of the presented computations, we shall use a homogeneous distribution of nodes with

$$h^a = \min_{\forall b} \left\{ |\mathbf{x}^a - \mathbf{x}^b| \right\} = \text{const} = h.$$

The radius of the interpolation domain and the radius of circular sub-domains have been taken as $r_i(\mathbf{x}^a) = 3.001 h^a$ and $r_s(\mathbf{x}^a) = 0.9 h^a$.

*Example 1*

The considered domain is a square $L \times L$ with applied tension load on the top, fixed bottom in vertical direction and tractions on the lateral sides are given by the analytical solution.
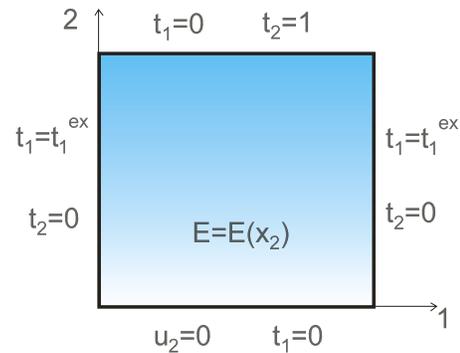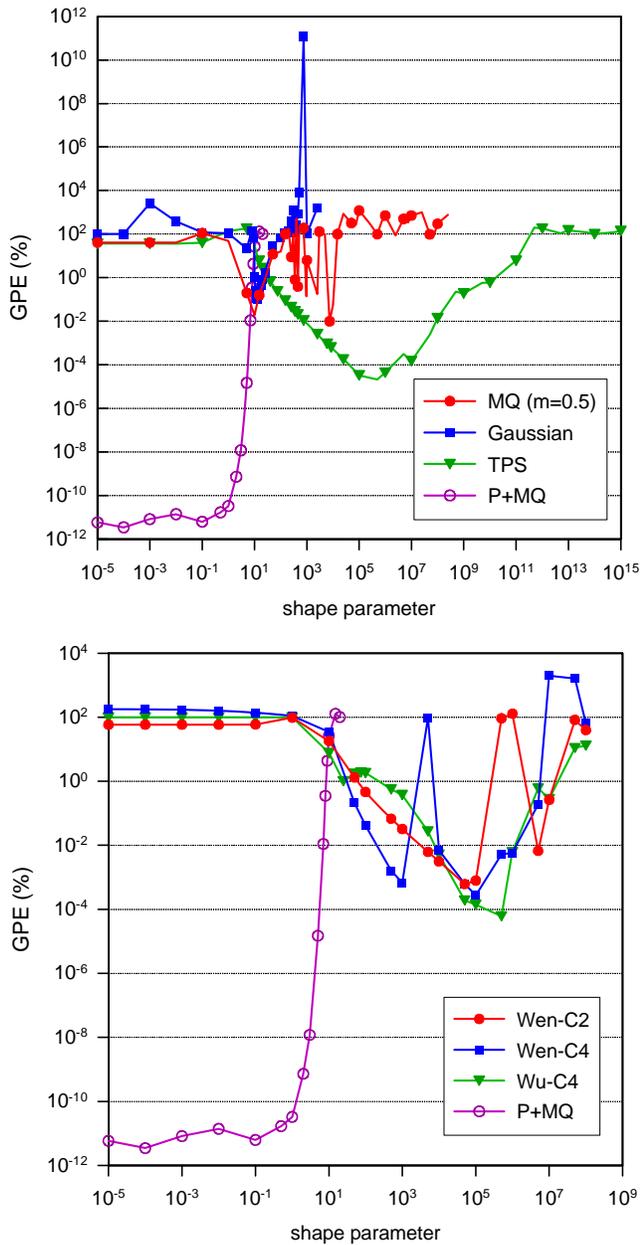


**Figure 2** : Square domain with prescribed boundary conditions

In this example, we consider exponential, power-law and trigonometric variation of the gradation function $f(\mathbf{x})$ with $\delta = 1$:

$$f(\mathbf{x}) = \exp(2\delta x_2/L),$$
$$f(\mathbf{x}) = (1 + \delta x_2/L)^2,$$
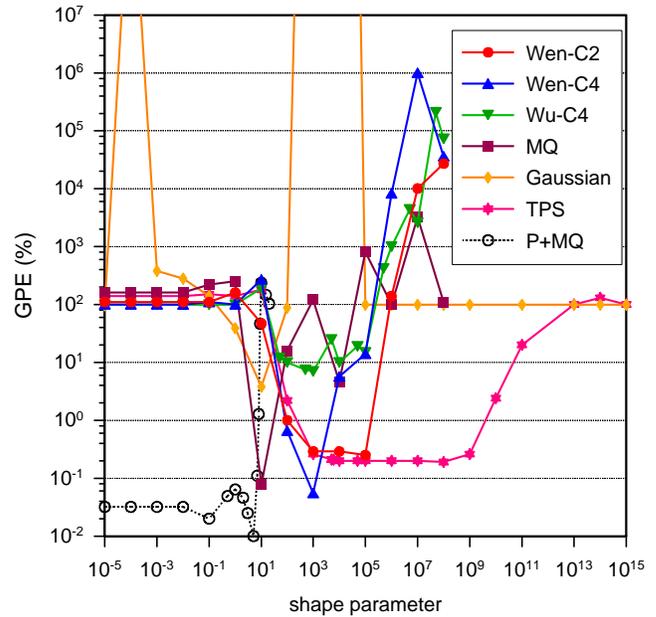$$f(\mathbf{x}) = (\cos(\delta x_2/L) + 2\sin(\delta x_2/L))^2 \qquad (21)$$

The exact solutions are available for each of the considered non-homogeneities [Sladek et al (2006)].

Fig. 3 shows the results in homogeneous elastic medium with using 121 uniformly distributed nodes and the integral equation treatment of traction boundary conditions in the LIE formulation for solution of BVPs. It can be seen that only in the case of combination of polynomials with multiquadrics there is a sufficiently wide interval for the shape parameter values resulting in stable and acceptable accuracy, while the use of PIM(RBF) approaches yields unacceptable accuracy of numerical results in the shape parameter stability zone. A similar study and comparisons have been carried out also in non-homogeneous media. It can be seen from Fig. 4 that only two of the investigated PIM(RBF), namely RBF ∈ {Wen - C2, TPS}, yield a sufficiently stable accuracy approaching the accuracy in the stability zone by the PIM(P+MQ).

**Figure 4** : Dependence of accuracy on the shape parameter of various RBFs used in the LIE approach in non-homogeneous elastic medium with exponentially graded Young's modulus



**Figure 3** : Dependence of accuracy on the shape parameter of various RBFs used in the LIE approach in homogeneous elastic medium

As regards the shape parameter sensitivity in the PIM(P+MQ) approach within the formulation utilizing collocation of the governing PDEs, Fig. 5 shows the results for both the homogeneous and exponentially graded elastic medium with using 441 uniformly distributed nodes. As compared with the sensitivity analysis for LIE formulation (Fig. 6), the differences are remarkable

in the non-homogeneous medium. Therefore, the accuracy in the PIM(P+MQ) – collocation approach can be strongly dependent on the choice of the shape parameter used in multiquadrics.

Now, we should like to compare the results of the convergence study in non-homogeneous elastic square domain (various gradations with $\delta = 1$) using various computational approaches and optimal values of the shape parameter. In the case of LIE-PIM(RBF) approaches, the presented results correspond to the exponential gradation of the Young modulus. It can be seen that the LIE – PIM(RBF) approaches obeying the integral force equilibrium on the Neumann part of the global boundary Fig. 7(b1) do not exhibit convergence of accuracy to zero with increasing the density of nodal points satisfactorily. Although the LIE – PIM(RBF) approaches obeying the traction boundary conditions at boundary nodes Fig. 7(b2) exhibit better convergence, only the PIM based on Wendland C4 compactly supported RBFs yields acceptable accuracy and convergence rate. However the shown results correspond to optimal choices of the shape parameters and the PIM(WEN-C4) is very sensitive with respect to the selection of the shape parameter. Con-

**Table 1** : Maximal % errors for displacements and stresses computed at interior points

| max % error | LIE-QE | | | LIE-PIM(P+MQ) | | | PIM(P+MQ)-colloc. | | |
|---|---|---|---|---|---|---|---|---|---|
| | exp. | power law | trig. | exp. | power law | trig. | exp. | power law | trig. |
| $u_2(L/2, x_2)$ | 0.10 | 0.15 | 0.58 | 0.042 | 0.042 | 0.24 | 0.22 | 0.34 | 1.28 |
| $\sigma_{22}(L/2, x_2)$ | 0.18 | 0.20 | 0.80 | 0.047 | 0.056 | 0.28 | 0.29 | 0.37 | 1.40 |
| $\sigma_{11}(L/2, x_2)$ | 0.27 | 0.22 | 1.08 | 0.026 | 0.038 | 0.30 | 0.29 | 0.34 | 1.30 |
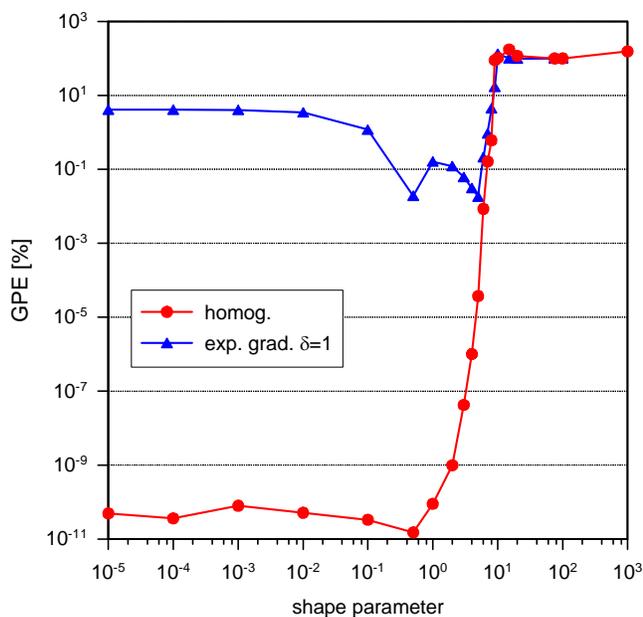


**Figure 5** : Dependence of accuracy on the shape parameter in the PIM(P+MQ) - collocation approach
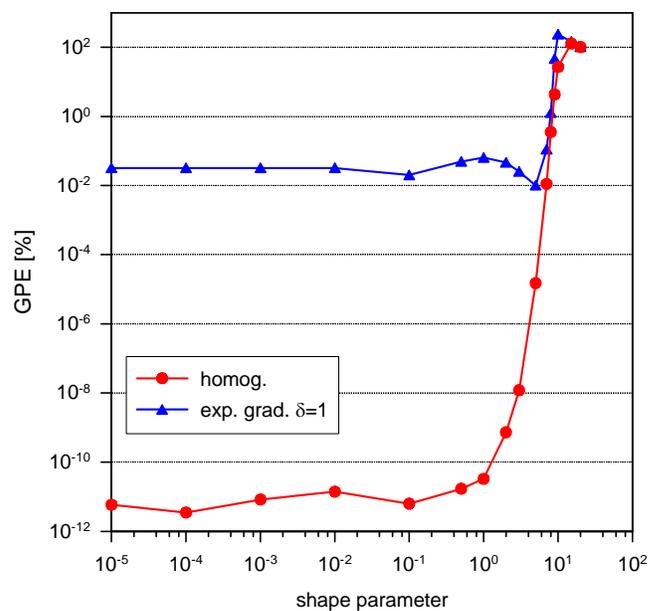


**Figure 6** : Dependence of accuracy on the shape parameter in the LIE-PIM(P+MQ) - approach (121 nodes)

cluding, none of the LIE – PIM(RBF) approaches can be considered reliable from the point of view convergence and stability of numerical results. Recall that in the case of PIM(P+MQ) collocation approach the convergence is achieved (Fig. 7(c)) but it can be instable with respect to selection of the shape parameter value. It may be interesting to compare the convergence of various meshless implementations with the convergence by LIE formulation combined with approximation based on standard quadrilateral quadratic elements as shown in Fig. 7(d).

Table 1 summarizes the maximal % errors of numerically computed displacements and stress tensor components at interior points along the vertical line $(L/2, x_2)$ by using

three different techniques:

(i) LIE with 400 standard quadrilateral quadratic elements (1281 nodes)

(ii) LIE-PIM(P+MQ) with 441 nodes

(iii) PIM(P+MQ)-collocation approach with 961 nodes

where the Young modulus is functionally graded according to exponential, power or trigonometric law (21) with $\delta = 1$.

Figure 8 shows the comparison of the CPU-times for solution of the BVP by four different approaches. It can be seen that differences between the CPU-times are decreasing by increasing the amount of nodes. This can be
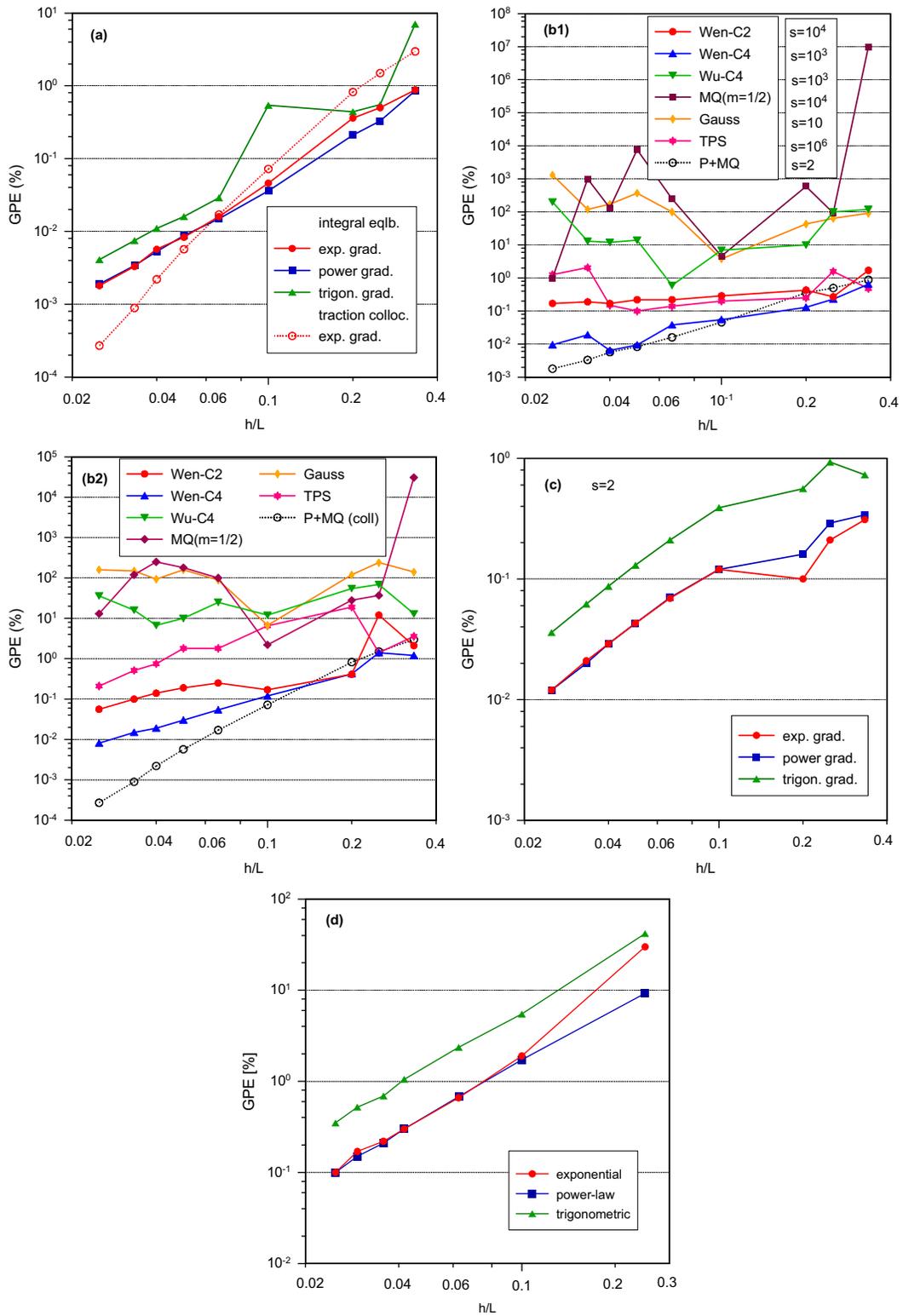
**Figure 7** : Convergence study in square domain using: (a) LIE-PIM(P+MQ); (b1) LIE-PIM(RBF) with integral equation treatment of traction b.c.; (b2) LIE-PIM(RBF) with collocation of traction b.c.; (c) PIM(P+MQ) collocation of governing PDEs; (d) LIE-QE
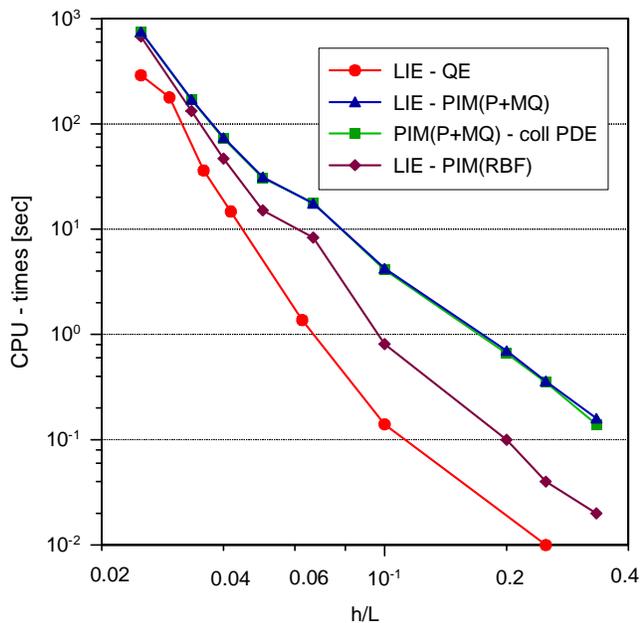
**Figure 8** : Comparison of CPU-times for solution of the BVP by the various approaches

explained by increasing rate of the time needed for solution of system of discretized equations with increasing the number of DOFs, while the time needed for numerical evaluation of shape functions at integration points is dominant in problems with small numbers of DOFs. Note that remarkable savings in the CPU-times with a simultaneous increase in accuracy have been achieved by using Gaussian integration over the angular variable on circular boundaries of sub-domains (with 12 integration points for $\varphi \in [0, 2\pi]$) as compared with the trapezoidal integration with splitting $[0, 2\pi]$ into 360 or 720 subintervals. Very low convergence rate has been observed in the latter approach with increasing the number of subintervals.

Up to now we presented the results obtained with using uniform distributions of nodes. Fig. 9 illustrates the stability of accuracy by the LIE-PIM(P+MQ) approach with respect to the distortion of the uniform distribution of nodes.

In addition to the BVP in the square domain, we have analysed also a hollow cylinder subject to interior pressure. The numerical results confirm completely the results obtained for the square domain.

## 6   Conclusions

The convergence, accuracy, numerical stability and computational efficiency have been investigated by solving two kinds of BVPs in square domain and radial cross-section of the hollow cylinder. The exact solutions are used as benchmark solutions and four numerical techniques are tested in applications to elasticity problems in functionally graded media:

(i) LIE supplemented with the approximation based on the standard quadrilateral quadratic elements

(ii) LIE supplemented with the meshless PIM based on the combination of polynomials and multiquadrics

(iii) LIE supplemented with the meshless PIM based on the RBFs alone

(iv) collocation of the governing PDE supplemented with meshless PIM based on the combination of polynomials and multiquadrics.
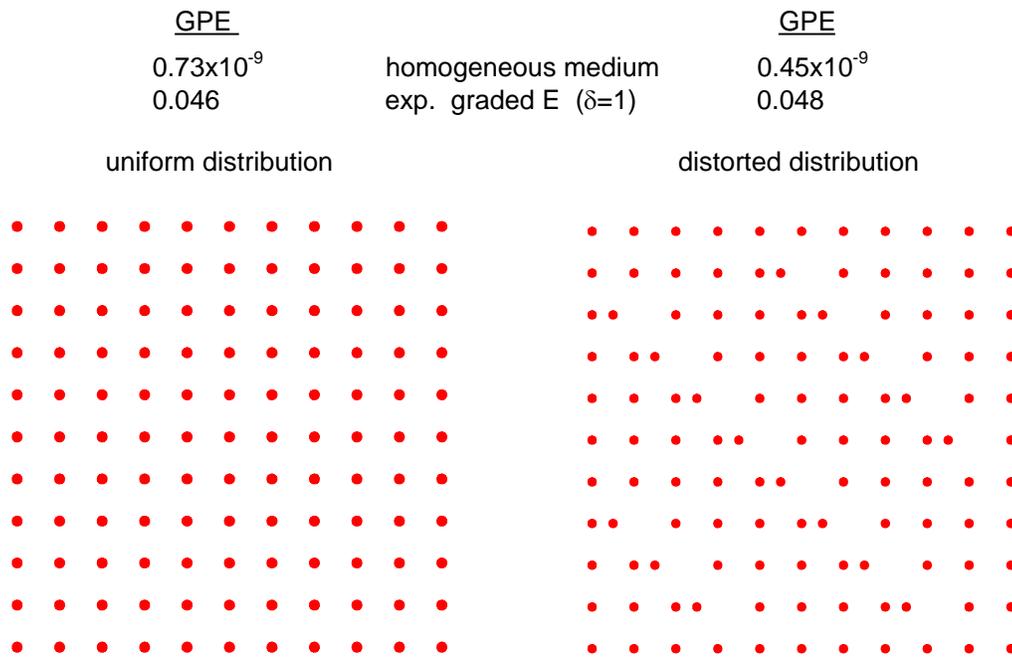
The LIE-PIM(RBF) approaches for various kinds of the RBFs can be considered as unreliable because of impossible simultaneous satisfaction of the numerical stability (because of the strong sensitivity of accuracy on the shape parameter selection) and acceptable convergence rate as well as accuracy of numerical results.

The PIM(P+MQ) – collocation PDE approach can be classified as not reliable because good accuracy and convergence can be achieved only for a narrow interval of the shape parameter values.

The LIE-PIM(P+MQ) approach as well as the LIE-QE approach exhibit numerical stability, reasonable accuracy and convergence to exact solution with increasing the density of nodes as well as stability with respect to a distortion of the uniform distribution of nodes.

The CPU-times consumed by meshless approaches are remarkably higher than the CPU-times consumed by the QE approach especially for low densities of nodes. The CPU-times converge to each other with increasing the density of nodes. The time required for preparation of boundary data is higher in the case of the QE approach.

GPE                                                                GPE

0.73x10$^{-9}$          homogeneous medium          0.45x10$^{-9}$
0.046                  exp.  graded E  ($\delta$=1)          0.048

uniform distribution                          distorted distribution

**Figure 9** : Illustration of the uniform and distorted distributions of 121 nodes in the square domain

**References**

**Atluri, S.N.; Shen, S**. (2002): *The meshless local Petrov-Galerkin (MLPG) method.* Tech Science Press, Encino, 429.

**Atluri, S.N.** (2004): *The meshless method (MLPG) for domain & BIE discretizations*, Tech Science Press, Forsyth, 677.

**Hardy, R.L.** (1990): Theory and applications of the multiquadrics-biharmonic method (20 years of discovery 1968-1988). *Comput Math Appl.*, vol. 19, pp. 163-208.

**Hughes, T.J.R.** (1987): *The finite element method. Linear static and dynamic finite element analysis.* Prentice-Hall, Inc.,Englewood Cliffs.

**Liu, GR.** (2003): *Mesh free methods, Moving beyond the finite element method.* CRC Press, Boca Raton, 691.

**Liu, GR. ; Gu, Y.T.** (2001): A local point interpolation method for stress analysis of two-dimensional solids. *Struct. Engrg. Mech.*, vol. 11, pp. 221-236.

**Liu, GR. ; Gu, Y.T.** (2003): A meshfree method: meshfree weak-strong (MWS) form method for 2-D solids. *Comput. Mechanics*, vol. 33, pp. 2-14.

**Rippa, S.** (1999): An algorithm for selscting a good value for the parameter c in radial basis functions interpolation. *Adv. Comput. Math.*, vol. 11, pp. 193-210.

**Sladek, V.; Sladek, J.; Tanaka, M.** (2005a): Local integral equations and two meshless polynomial interpolations with application to potential problems in non-homogeneous media. *CMES: Computer Modeling in Engineering & Sciences*, vol. 7, pp. 69-83.

**Sladek, V.; Sladek, J.; Zhang, Ch.** (2005b): Local integro-differential equations with domain elements for numerical solution of PDE with variable coefficients. *Jour Engn Mathematics*, vol. 51, pp. 261-282.

**Sladek, V.; Sladek, J.; Zhang, Ch.** (2006): A meshless Point Interpolation Method for Local Integral Equations in elasticity of non-homogeneous media. In: *Advances in the Meshless Method (J. Sladek, V. Sladek, S.N. Atluri, eds.),* Tech Science Press, Forsyth, 2006.

**Wang, J.G.; Liu, G.R.** (2002): On the optimal shape parameters of radial basis functions used for 2-D meshless methods. *Comput. Meth. Appl. Mech. Engrg.*, vol 191, pp. 2611-2630.

**Xiao, J.R.; McCarthy, M.A.** (2003): A local Heaviside weighted meshless method for two-dimensional solids using radial basis functions. *Comput. Mechanics*, vol. 31, pp. 301-315.

**Xiao, J.R.** (2004): Local Heaviside weighted MLPG meshless method for two-dimensional solids using compactly supported radial basis functions. *Comput. Meth. Appl. Mech. Engrg.*, vol. 193, pp. 117-138.

**Zhou, X.; Hon, Y.C.; Li, J.** (2003): Overlapping domain decomposition method by radial basis functions. *Appl. Numer. Math.*, vol. 44, pp. 241-255.